© 2026. Published by The Company of Biologists | Journal of Cell Science (2026) 139, jcs264962. doi:10.1242/jcs.264962

RESEARCH ARTICLE

The fungal virulence factor PefD activates sleep neurons of *Caenorhabditis elegans*

Anna-Lena Klemke[§], Xiaodi Hu[§,*], Pietrina Steudel, Nicole Wernet, Valentin Wernet[‡], Elke Wohlmann and Reinhard Fischer[¶]

ABSTRACT

Nematode-trapping fungi such as *Arthrobotrys flagrans* employ sophisticated strategies to immobilize and digest their prey. A critical, yet poorly understood, step in this interaction is the induction of prey paralysis following capture. Here, we characterize putative effector D (PefD), a small secreted protein from *A. flagrans*. We demonstrate that *pefD* expression is specifically upregulated during the early and middle stages of infection of *Caenorhabditis elegans* (12–24 h post inoculation) and PefD localizes to the infection bulb within the nematode. Deletion of *pefD* significantly delayed the paralysis of *C. elegans*, whereas its overexpression accelerated the process. Through heterologous pan-neuronal expression in *C. elegans*, we show that PefD directly attenuates host locomotion and significantly enhances the activity of the sleep-promoting RIS interneuron. Unlike other effectors such as NipA or CyrA, PefD specifically modulates neuronal activity patterns without inducing general neurodegeneration. Our results identify PefD as a key virulence factor that hijacks the endogenous sleep induction circuitry of the host to facilitate rapid prey immobilization.

KEY WORDS: Virulence factor, Effector protein, Small secreted protein

INTRODUCTION

In nature, the survival of a predator depends on its ability to efficiently capture prey while minimizing energy expenditure and risk of injury. A near-universal strategy to achieve this is paralysis. In the animal kingdom, venomous predators like the Formosan krait (*Bungarus multicinctus*) or the Brazilian wandering spider (*Phoneutria nigriventer*) utilize complex cocktails of neurotoxic proteins, such as β-bungarotoxin, to disrupt neuromuscular transmission and ion channel function (Gomez et al., 2002; Gundersen et al., 1981; Ranawaka et al., 2013; Tasoulis and Isbister, 2017). This chemical control allows the predator to secure struggling prey, prevent its escape and, in some cases, preserve it for later consumption.

This biological challenge is not limited to animals; it is shared by nematode-trapping fungi. Comparative genomics of nematode-trapping fungi reveals that carnivory evolved through gene family expansions and contractions and horizontal gene transfer, enabling adaptation to carbon-rich, nitrogen-poor environments (Fan et al., 2025). In particular, genes encoding adhesive proteins, cysteine-rich secretory proteins and proteases, which are associated with nematode capture, infection and consumption, are expanded, alongside genes involved in cellulose degradation and amino acid uptake. Species such as *Arthrobotrys flagrans* must immobilize nematodes to prevent them from damaging the fungal mycelia or escaping the adhesive three-dimensional trapping networks (Jiang et al., 2017). Trap formation and ring closure are interesting phenomena and rely on the interplay between the cytoskeleton, cell-end marker proteins and cell-to-cell communication (Kriegler et al., 2025; Wernet et al., 2023, 2022). The interaction is robustly regulated through chemical communication with fungal- and nematode-derived molecules (Hsueh et al., 2017, 2013; Hu et al., 2024; Kuo et al., 2024).

Following capture, the fungus penetrates the cuticle of the nematode and forms an infection bulb inside the host. This bulbous structure represents a swelling of the invading hypha from where trophic hyphae grow out to colonize the prey (Vidal-Diez de Ulzurrun and Hsueh, 2018). Although the role of lytic enzymes and proteases in the later stages of digestion is well documented (Emser et al., 2025; Lin et al., 2023; Youssar et al., 2019), the precise mechanisms of initial penetration and subsequent paralysis remains unclear. In *Arthrobotrys oligospora*, a close relative of *A. flagrans*, nematode paralysis occurs within 20 min of capture, coinciding with the activation of the RIS and ALA neurons – interneurons in *Caenorhabditis elegans* that induce stress-induced sleep (Hill et al., 2014; Lin et al., 2025; Steuer Costa et al., 2019; Turek et al., 2013).

Recent research suggests that small secreted proteins (SSPs) serve as critical virulence factors during this process. Of the ∼200 SSPs identified in *A. flagrans*, 117 are predicted effectors (Fischer and Requena, 2022; Youssar et al., 2019). These effectors exhibit distinct spatiotemporal expression: early-stage effectors such as NipA facilitate cuticle penetration, whereas middle-stage effectors such as CyrA, produced at the infection bulb, contribute to paralysis (Emser et al., 2024; Wernet et al., 2021). Furthermore, the fungal attack can hijack host pathways, such as inducing *C. elegans* neuropeptide-like proteins (e.g. Nlp-27) to accelerate neurodegeneration (Pop et al., 2024).

In this study, we characterize a novel SSP from *A. flagrans* termed putative effector D (PefD). PefD is upregulated during infection, localizes specifically to the infection bulb and plays a significant role in prey paralysis. Furthermore, we demonstrate that pan-neuronal expression of PefD in *C. elegans* increases the activity of the sleep-promoting RIS neuron, suggesting a direct link between this fungal effector and the induction of host paralysis.

RESULTS

PefD is a SSP

Bioinformatic analysis of the *A. flagrans* secretome identified over 100 potential SSPs (Sperschneider et al., 2018; Youssar et al., 2019).

Karlsruhe Institute of Technology (KIT) - South Campus, Institute for Applied Biosciences, Department of Microbiology, Fritz-Haber-Weg 4, D-76131 Karlsruhe, Germany.
*Present address: Key Laboratory of Agricultural Environmental Microbiology, Ministry of Agriculture and Rural Affairs, Department of Microbiology, College of Life Sciences, Nanjing Agricultural University, Nanjing 210095, Jiangsu, PR China.
‡Present address: BASF SE, Carl-Bosch-Strasse 38, 67056 Ludwigshafen, Germany.

§These authors contributed equally to this work

¶Author for correspondence (reinhard.fischer@kit.edu)

R.F., 0000-0002-6704-2569

Handling Editor: Guangshuo Ou
Received 14 April 2026; Accepted 13 May 2026

Journal of Cell Science (2026) 139, jcs264962. doi:10.1242/jcs.264962

Among these, the candidate Dfl_005559 (RVD83782.1) – designated here as PefD – showed a high effector probability of 0.94. The presence of a 60 nt intron in *pefD* was experimentally validated by RNA sequencing, as evidenced by multiple split reads spanning the exon–exon junction (Fig. S1A). The resulting 72-amino acid protein includes a predicted N-terminal signal peptide [amino acids (aa) 1–28] (GenBank PZ405203). Orthologs of PefD are restricted to nematode-trapping fungi. Structural modeling via AlphaFold 3 suggests that PefD contains four conserved cysteines forming two disulfide bridges, likely providing structural stability to the mature protein (Fig. 1A,B) (Abramson et al., 2024). The 1.5 kb genomic upstream sequence of the *pefD* open reading frame (ORF) contains two putative upstream ORFs (uORFs), encoding peptides with 57 and 35 amino acids, respectively (Fig. S1B).

To experimentally validate the secretion of PefD, we utilized a laccase-based reporter assay [2,2′-azino-bis-(3-ethylthiazoline-6-sulfonate) (ABTS) assay]. We fused the *Aspergillus nidulans* laccase C (lacking its native signal peptide) C-terminally to PefD and expressed the construct under the constitutive *gpdA* promoter. Successful secretion of the fusion protein leads to oxidation of ABTS in the medium, producing a characteristic blue halo. After 2 days of growth on potato dextrose agar (PDA) plates supplemented with 1 mM ABTS, colonies expressing the PefD–laccase fusion showed a distinct blue color change in the surrounding medium. In contrast, neither the wild-type (WT) nor the control strain (expressing laccase fused to PefD lacking the signal peptide) exhibited a color change, confirming that the PefD signal peptide is fully functional and drives protein secretion (Fig. 1C).

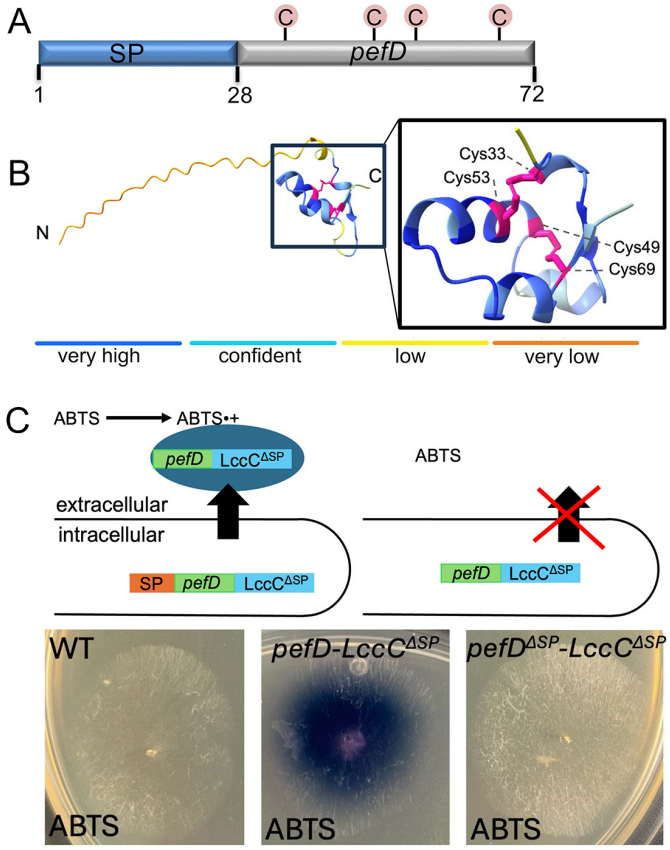


Fig. 1. PefD is a small secreted cysteine-rich protein. (A) Scheme of PefD from *Arthrobotrys flagrans*. The 72-amino-acid protein contains a predicted signal peptide [SP; amino acids (aa) 1–28; blue] at the N-terminus and four cysteine residues (C33, C 49, C53, C69; pink) in the remaining sequence (aa 29–72). (B) Predicted three-dimensional structure of PefD modeled using AlphaFold 3. The color gradient indicates the predicted local distance difference test (pLDDT) confidence scores: very high, pLDDT>90; confident, 90>pLDDT>70; low, 70>pLDDT>50; very low, pLDDT<50. The cysteine residues are highlighted in dark pink. (C) Laccase assay of PefD. Full-length *pefD* was C-terminally fused to a laccase from *Aspergillus nidulans* lacking its own SP and expressed under control of the constitutive *gdpA* promoter. The SP of PefD mediates secretion of the PefD–laccase fusion protein, leading to oxidation of ABTS in the medium, which results in the blue color. Deletion of the SP from PefD (*pefD*$^{\Delta SP}$) inhibits laccase secretion (upper panel). Wild-type (WT) and transformants were incubated on potato dextrose agar (PDA) plates containing 1 mM ABTS for 2 days at 28°C. Images represent three independent experiments.

pefD expression is upregulated during the infection of *C. elegans*

A hallmark of fungal effectors is their stage-specific expression during the infection process. To characterize the transcriptional dynamics of *pefD*, we performed quantitative real-time PCR (qRT-PCR) by comparing uninduced vegetative mycelia with nematode-induced mycelia at 12, 24 and 40 h post inoculation (hpi). In uninduced mycelia, *pefD* transcript levels remained at baseline [12 h: $(7.0\pm1.7)\times10^{-4}$; 24 h: $(4.4\pm1.3)\times10^{-4}$; indicated as mean±s.d.]. In contrast, induction by *C. elegans* led to a significant upregulation at the early and middle stages of infection, with relative expression reaching $(6.0\pm0.78)\times10^{-3}$ at 12 hpi and $(5.0\pm1.0)\times10^{-3}$ at 24 hpi (Fig. 2A). By 40 hpi, expression levels significantly declined, suggesting that *pefD* primarily functions during the initial trapping and colonization phases.

To resolve the spatial pattern of this induction, we utilized a promoter–reporter assay. A 1.5 kb sequence upstream of *pefD* was fused to an *h2B-mCherry* construct to label nuclei where the *pefD* promoter is active, while a construct encoding a constitutively expressed histone (*h2B-GFP*) served as an internal control for nuclear localization and general metabolic activity. Although the GFP signal remained uniform across all conditions [uninduced: 65±15; induced: 60±14; values show the mean±s.d. of corrected total nuclear fluorescence (CTNF)], the mCherry signal was significantly more intense in induced mycelia (225±53) compared to that in uninduced controls (112±26) (Fig. 2B,C). Detailed spatial analysis revealed that this upregulation is specific to infection structures. There was no significant difference in mCherry intensity between vegetative hyphae of uninduced (112±26) and induced (123±38) samples (Fig. 2D). However, within induced cultures, *pefD* promoter activity was significantly higher in specialized infection structures, such as traps and trophic hyphae (162±75), compared to the surrounding vegetative hyphae (123±38) (Fig. 2E). These results demonstrate that *pefD* is specifically induced in response to nematodes and is spatially concentrated at the site of fungal-prey interaction.

PefD localizes to the infection bulb

Beyond temporal regulation, the spatial distribution of an effector is crucial for understanding its functional role. To track PefD during the infection process, we generated fusion proteins with GFP or mCherry under the control of the native *pefD* promoter. Although no distinct fluorescence was detectable in vegetative hyphae, PefD localized to vesicle-like structures concentrated at the inner rim of the traps. This localization was strictly dependent on the N-terminal signal peptide: a truncated PefD (lacking the signal peptide) remained cytoplasmic, whereas the signal peptide alone was sufficient to target the fluorophore to these vesicle-like compartments (Fig. 3A). Interestingly, although *pefD* mRNA and promoter activity were detectable at basal levels in vegetative mycelia (Fig. 2), the protein

Journal of Cell Science (2026) 139, jcs264962. doi:10.1242/jcs.264962

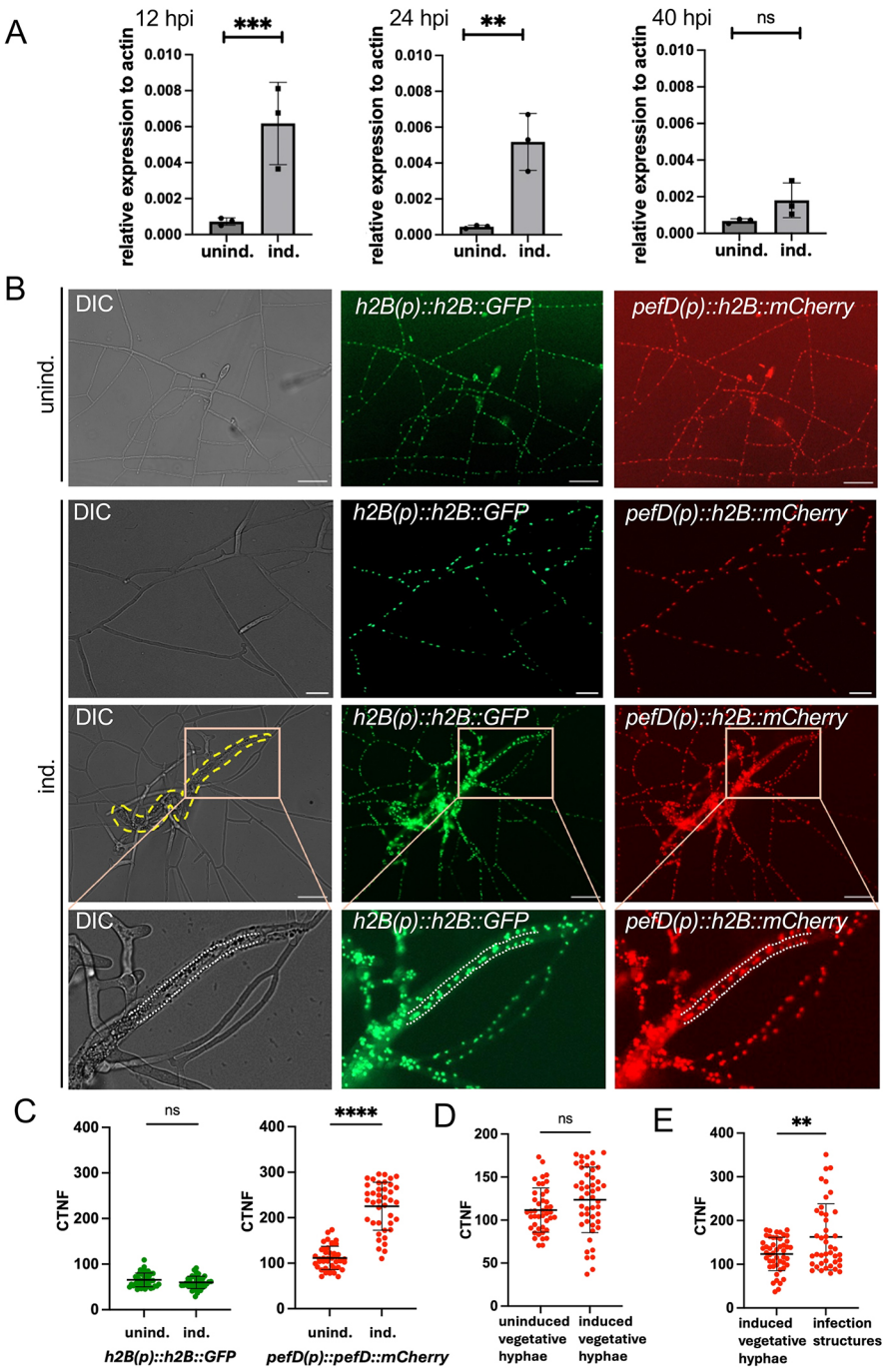


Fig. 2. *pefD* is upregulated during the infection process. (A) Relative expression of *pefD* determined by qRT-PCR analysis of RNA extracted from uninduced mycelia grown on low-nutrient agar (LNA) plates and co-incubated mycelia with nematodes shows an upregulation in the middle stage of the infection process. Samples were collected at three different timepoints after the induction with nematodes [12, 24 and 40 h post inoculation (hpi)]. The expression was normalized to actin. The error bars show the standard deviation and statistical significance was determined using an unpaired two-tailed Student's *t*-test. (B) Spatial analysis of *pefD* expression using a transcriptional reporter assay. The *pefD* promoter [*pefD(p)*] was fused to *h2B* and *mCherry* and, as a control, *h2B* with its native promoter [*h2B(p)*] was fused to *GFP*. Images of induced and uninduced mycelia were taken at 24 hpi. The upper panel shows uninduced mycelia, and the lower panels show induced mycelia containing both vegetative hyphae and infection structures. Representative examples of both are shown (top, induced vegetative hyphae; middle and bottom, infection structures). A captured nematode is indicated with a yellow dashed line in the differential interference contrast (DIC) image. Magnified views of the boxed region containing the captured nematode are shown, and dashed lines show the trophic hyphae inside the nematode. Scale bars: 50 µm. (C) Quantification of corrected total nuclear fluorescence (CTNF) of GFP (left) and mCherry (right) in the nuclei of induced and uninduced mycelia. GFP signal was comparable in all nuclei of induced and uninduced mycelia, whereas the mCherry signal was higher in induced mycelia than in uninduced mycelia. The signal was higher in traps and in trophic hyphae. *n*=43, *h2B(p)::h2B::GFP*, uninduced; n=39, *h2B(p)::h2B::GFP*, induced; *n*=43, *pefD(p)::h2B::mCherry*, uninduced; *n*=40, *pefD(p)::h2B:mCherry*, induced. (D) Quantification of CTNF of mCherry in nuclei of induced and uninduced vegetative hyphae. The mCherry signal was comparable in induced and uninduced vegetative hyphae. *n*=43, uninduced; *n*=48, induced. (E) Quantification of CTNF of mCherry in nuclei of induced vegetative hyphae and infection structures such as traps and trophic hyphae. The mCherry signal was higher in the infection structures than in the induced vegetative hyphae. *n*=48, vegetative hyphae; *n*=42, infection structures. In C–E, nuclei were measured using ImageJ. Bars indicate mean ±s.d. Significance was determined using an unpaired two-tailed Student's *t*-test. ns, not significant, $P>0.05$; **$P\leq0.01$; ***$P\leq0.005$; ****$P\leq0.0001$.

itself remained undetectable until trap formation (Fig. 3A). This discrepancy suggests a significant layer of translational or post-transcriptional control, a phenomenon documented in other filamentous fungi in which 5′ regulatory elements, such as uORFs, modulate translation efficiency (Hood et al., 2009). Whether the two uORFs detected in the putative promoter region of *pefD* are of relevance for such a regulation remains to be determined (Fig. S1A).

During the infection of *C. elegans*, PefD was specifically localized within the infection bulb, a bulbous swelling formed by the penetrating hypha inside the nematode after cuticle penetration, but was notably absent from the subsequently emerging trophic hyphae (Fig. 3B,E). Dual-localization experiments confirmed this spatial specificity: PefD signals showed a clear overlay with the known middle-stage effector CyrA, which also localizes to the infection bulb (Fig. 3C). In contrast, no overlap was observed with the early-stage effector NipA, which is secreted at the penetration site outside the nematode (Fig. 3D). These results indicate that PefD acts as a middle-stage effector, functioning after cuticle penetration but before extensive colonization of the prey.

To investigate the fate of PefD within the host, we heterologously expressed the protein in *C. elegans* under the constitutive, pan-tissue promoter *eft-3*. PefD accumulated in the coelomocytes – scavenger cells that endocytose proteins from the pseudocoelomic fluid (Wernet et al., 2021) (Fig. 3F). This accumulation suggests that PefD is effectively secreted into the body cavity of the host and

Journal of Cell Science

Journal of Cell Science (2026) 139, jcs264962. doi:10.1242/jcs.264962

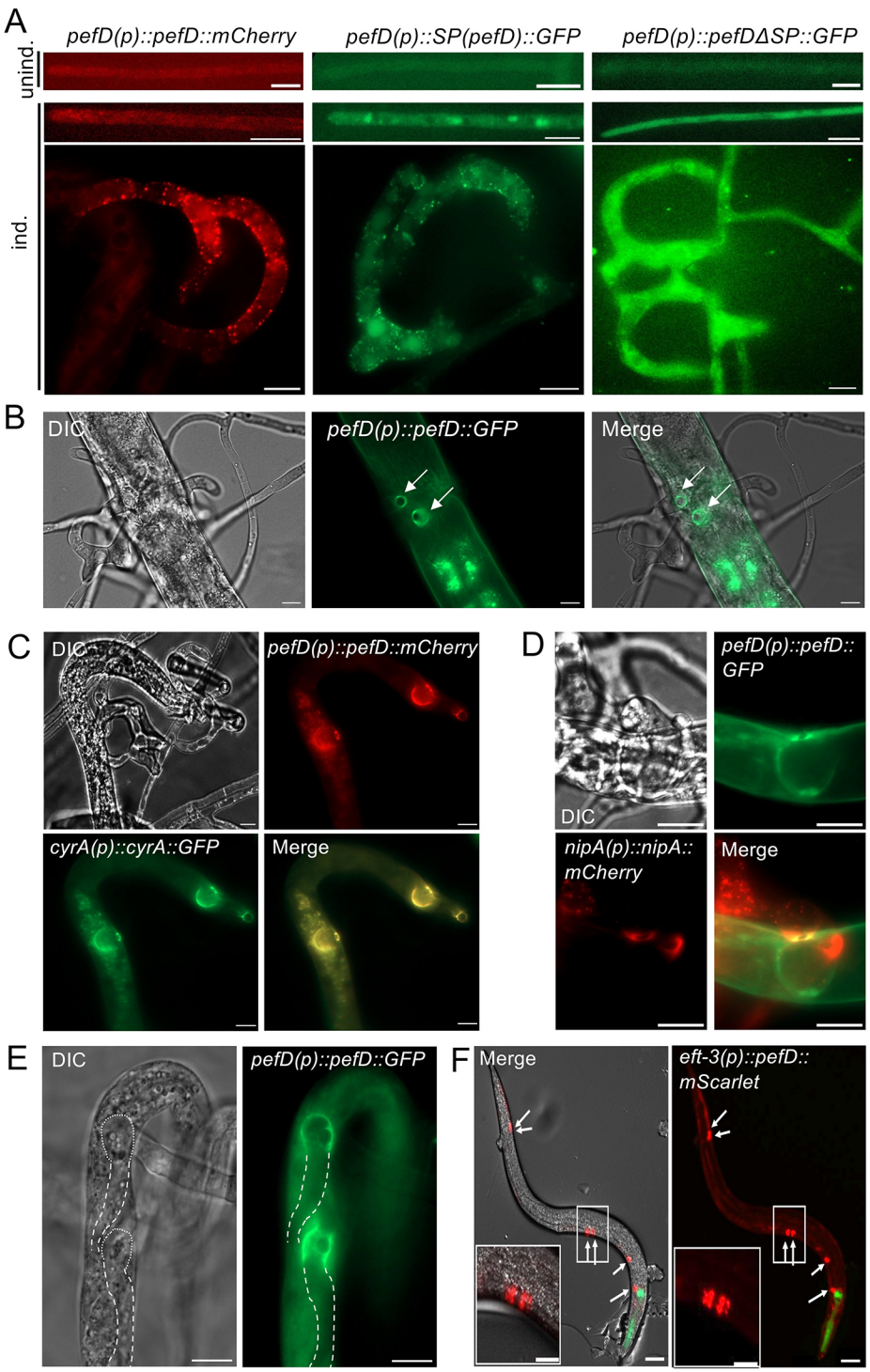


Fig. 3. PefD localizes at the infection bulb. Fluorescence microscopy of *A. flagrans* expressing different PefD fusion constructs. (A) PefD fused to mCherry under control of its native promoter localized to vesicle-like structures concentrated at the inner rim of the traps. In vegetative hyphae, no distinct fluorescence signal could be detected in induced or uninduced stadium. Expression of the signal peptide (SP) of PefD fused to GFP produced a similar fluorescence pattern, whereas deletion of the SP resulted in cytoplasmic localization in the traps and the induced vegetative hyphae. (B) PefD localized at round intracellular structures corresponding to the infection bulb (white arrows), a bulbous swelling formed by the penetrating hypha inside a trapped nematode after cuticle penetration. (C) Colocalization studies of PefD and CyrA show overlapping fluorescence signals at the infection bulb. (D) NipA and PefD show partial colocalization. NipA localized predominantly at the penetration site, whereas PefD was also detected in the infection bulb. (E) PefD localized only at the infection bulb (indicated by dotted white lines) and not in the trophic hyphae (dashed white lines). (F) When *pefD* was heterologously expressed in *C. elegans* under the control of the *eft-3* promoter, it localized in the coelomocytes (white arrows and magnified views) – specialized scavenger cells that take up secreted proteins from the pseudocoel – suggesting that secreted PefD can freely diffuse in the host tissue. Scale bars: 10 µm (A–E); 50 µm (F); 20 µm (insets in F). Images represent three independent experiments.

distributed through the pseudocoel, rather than accumulating in specific host tissues.

Deletion of *A. flagrans pefD* delays nematode paralysis

The specific expression of *pefD* during the middle stage of infection (12–24 hpi) and its localization within the infection bulb suggest a role in host immobilization or the suppression of the immune response in the nematode. To investigate the molecular function of PefD, we generated *A. flagrans* deletion (Δ*pefD*) and overexpression (OE::*pefD*) strains. In the deletion strain, the *pefD* ORF was replaced with a hygromycin-resistance cassette via homologous recombination. For overexpression, *pefD* was fused to the constitutive *A. nidulans oliC* promoter (Fig. 4A). Successful deletion was confirmed by Southern blotting and analytical PCR (Fig. 4B). Both modified strains exhibited vegetative growth and morphology indistinguishable from those of the WT strain (Fig. 4C). To test whether PefD facilitates prey immobilization, we performed virulence assays with these fungal strains, measuring the time to complete paralysis. The assay period was defined from the initial contact with the trap (capture) to the complete cessation of nematode movement (Movie 1). Although the WT strain required approximately 86±35 min (n=35) to paralyze the prey, the Δ*pefD* strain took significantly longer, requiring

Journal of Cell Science

Journal of Cell Science (2026) 139, jcs264962. doi:10.1242/jcs.264962

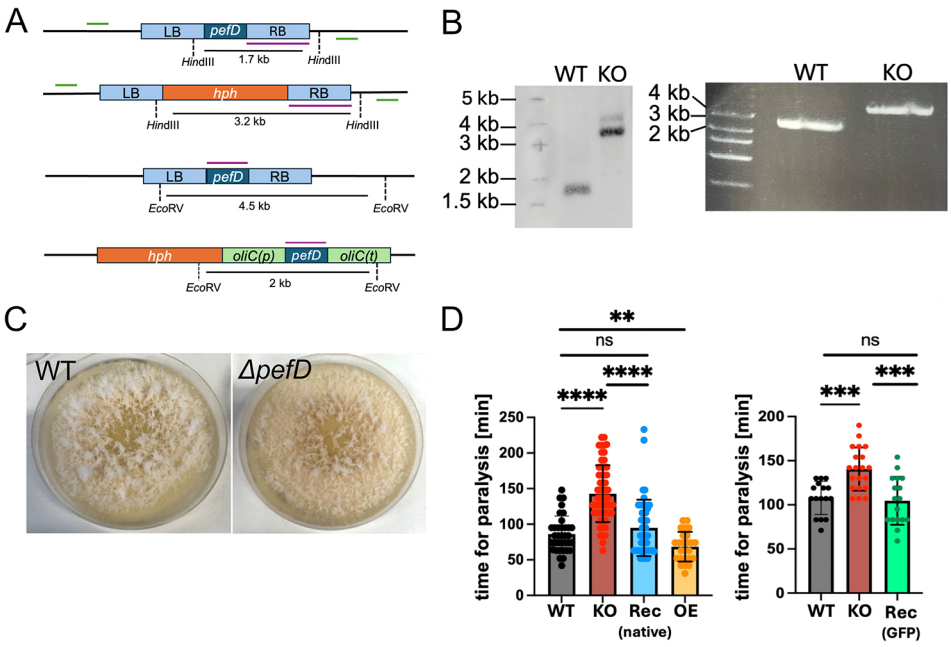


Fig. 4. Deletion of *pefD* leads to longer paralysis of captured nematodes. (A) Scheme of the *pefD* deletion and overexpression constructs. For the deletion strain, the *pefD* open reading frame was replaced by a hygromycin resistance cassette (*hph*) via homologous recombination using flanking regions (LB, left border; RB, right border). Positions of Southern blot probes (purple), analytic PCR oligonucleotides (green), restriction sites and expected fragment sizes are indicated. (B) Verification of the representative *pefD* deletion mutant (knockout or KO) by Southern blot (left) and analytical PCR (right). Genomic DNA digested with HindIII produced fragments of the expected size for WT (1.7 kb) and the deletion mutant (3.2 kb). PCR amplification yielded fragments of approximately 2 kb for the WT and 4.5 kb for the deletion mutant, confirming correct integration. (C) Colony morphology of the WT and *pefD* deletion strain (*ΔpefD*) grown on PDA plates for 7 days at 28°C. No obvious differences in growth phenotype were observed. (D) Quantification of the paralysis time of captured nematodes. The deletion strain took longer to paralyze the nematodes than the WT strain and the overexpression strain was faster with the paralysis. Shown are WT, a representative *pefD* deletion strain (KO), the overexpression strain (OE), and the complemented strains expressing *pefD* either with the native promoter and terminator (Rec native) or as a GFP fusion (Rec GFP). Each dot represents an individual measurement: WT, *n*=35; KO, *n*=59; OE, *n*=25; Rec native, *n*=48; Rec GFP, *n*=26. Bars indicate mean±s.d. Statistical significance was determined using an unpaired two-tailed *t*-test. ns, not significant, $P>0.05$; $^{**}P\leq0.01$; $^{***}P\leq0.005$; $^{****}P\leq0.0001$.

141±39 min (*n*=59). Conversely, the overexpression strain accelerated paralysis, reducing the time to 69±21 min (*n*=25). The causal role of *pefD* was further confirmed through genetic complementation: reintroducing a WT copy (95±40 min; *n*=48) or a *pefD-GFP* fusion (104±27 min; *n*=26) into the Δ*pefD* background restored paralysis kinetics to near-WT levels (Fig. 4D). These results demonstrate that PefD is a critical virulence factor that directly contributes to the rapid paralysis of *C. elegans* during the infection process.

Heterologous pan-neuronal expression of PefD attenuates *C. elegans* locomotion

As the natural secretion of PefD during infection might exert highly localized effects, we utilized heterologous expression within *C. elegans* to amplify and characterize its impact on host physiology. Given that PefD-mediated paralysis likely targets the host nervous system, we expressed *pefD* [both with and without its signal peptide (ΔSP)] pan-neuronally under the control of the *rab-3* promoter. This promoter drives expression specifically in neurons, in contrast to the broadly active pan-tissue *eft-3* promoter used above. These constructs were injected into *C. elegans* N2 as extrachromosomal arrays, using *myo-2(p)::tDTomato* [where '*(p)*' indicates promoter] as a transformation marker. For comparison, the previously characterized effectors NipA and CyrA were similarly expressed.

Initial observations revealed that each PefD-expressing line exhibited markedly slower locomotion compared to WT N2 worms. To quantify this phenotype, we recorded 1-min videos of individual nematodes and traced their movement using ImageJ (Fig. 5A; Movie 2). Nematodes expressing either PefD or PefDΔSP moved significantly slower and covered shorter distances than WT N2 worms (Fig. 5B,C). Specifically, the average speed of WT N2 was 5.9±1.0 µm/s (*n*=10; indicated as mean±s.d.), whereas PefD-expressing worms averaged a speed of 1.3±0.8 µm/s (*n*=11) and PefDΔSP-expressing worms averaged 1.5±0.6 µm/s (*n*=9). The total distance traveled mirrored these findings: WT N2 nematodes covered a distance of 356±61 µm (*n*=10; indicated as mean±s.d.), whereas the PefD- and PefDΔSP-expressing lines traveled only 80±47 µm (*n*=11) and 89±35 µm (*n*=9), respectively. Notably, the reduction in locomotion was significantly more pronounced in PefD-expressing lines than in those expressing NipA or CyrA, regardless of the presence of a signal peptide. These data demonstrate that PefD possesses potent neuroactive properties capable of inhibiting host locomotion independently of the natural fungal delivery process.

Heterologous expression of PefD enhances RIS neuron activity

Based on the observed paralysis phenotype, we hypothesized that PefD interacts with the *C. elegans* nervous system, specifically targeting sleep-promoting neurons such as RIS. In *A. oligospora*, RIS activation marks the onset of nematode paralysis (Lin et al., 2025). To test this, we expressed *pefD* (with and without signal peptide) pan-neuronally in a *C. elegans* strain (sPS01) expressing the Ca^{2+} indicator GCaMP6 in the RIS neuron under the *flp-11* promoter. Parallel control lines expressing *nipA* or *cyrA* were also established.

Journal of Cell Science (2026) 139, jcs264962. doi:10.1242/jcs.264962

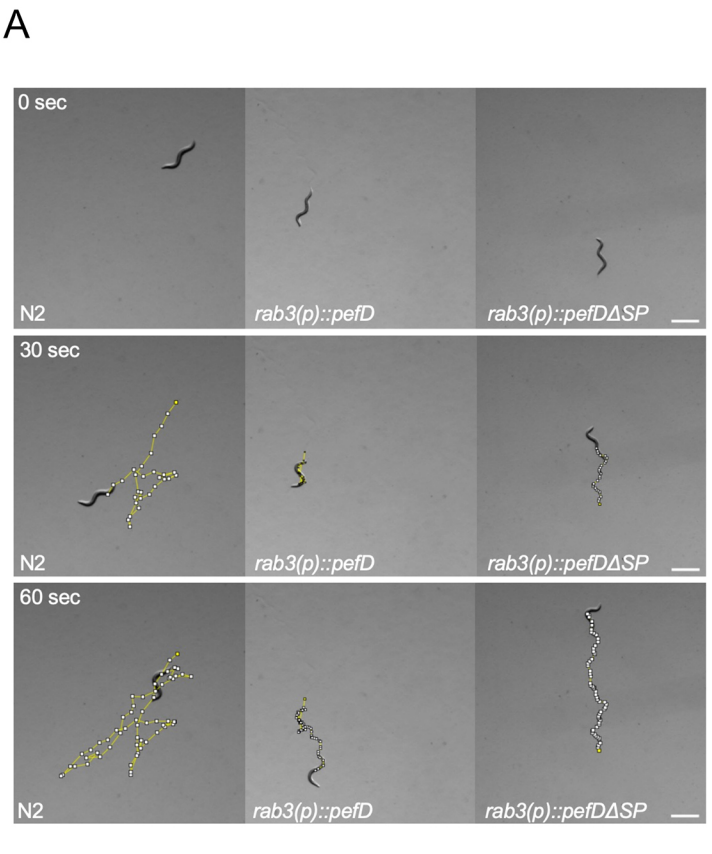


Fig. 5. Pan-neuronal expression of *pefD* reduces locomotion in *C. elegans*. (A) Representative snapshots from the locomotion assays of *C. elegans*. Frames show worms at 0, 30 and 60 s, and yellow dotted lines show movement of the nematode. WT N2 is compared to lines expressing *pefD* or *pefD* without the signal peptide (SP) under the pan-neuronal *rab-3* promoter. Scale bars: 100 µm. (B) Quantification of the total distance traveled within 1 min. Worms expressing *pefD* or *pefDΔSP* traveled less distance than the WT. Additional lines expressing *nipA*, *nipAΔSP*, *cyrA* and *cyrAΔSP* are shown for comparison. (C) Average speed of the analyzed strains. Neuronal expression of *pefD* or *pefDΔSP* resulted in reduced movement speed compared to that of WT N2. All genes were expressed under the *rab-3* promoter. Each dot represents an individual animal: N2, *n*=10; *pefD*, *n*=11; *pefDΔSP*, *n*=9; *nipA*, *n*=10; *nipAΔSP*, *n*=10; *cyrA*, *n*=12; *cyrAΔSP*, *n*=11. Bars indicate mean±s.d. Statistical significance was determined using a Kruskal–Wallis test with Dunn's post hoc test. *$P \leq 0.05$; **$P \leq 0.01$; ****$P \leq 0.0001$.

Initial structural analysis confirmed that the presence of PefD did not damage the morphology of the RIS neuron (Fig. 6A). To quantify neuronal activity, we performed live Ca^{2+} imaging on immobilized nematodes (Fig. 6B). Relative GCaMP6 fluorescence was normalized against a 1-min baseline to determine overall activity patterns. Our results show that both PefD- and PefDΔSP-expressing lines exhibited significantly higher overall RIS activity compared to that in sPS01 and other effector controls (Fig. 6C–E).

Statistical analysis of three parameters – mean GCaMP6 fluorescence, net activity (area under the curve) and frequency of positive peaks – confirmed this trend. The mean fluorescence was markedly higher in lines expressing PefD (0.13±0.3; *n*=8; indicated as mean±s.d.) and PefDΔSP (0.02±0.4; *n*=10) compared to the sPS01 control (−0.5±0.17; *n*=10). Similarly, net activity was elevated (PefD: 3.9±10; PefDΔSP:0.67±10; indicated as mean±s.d.) relative to that of the control (−14.33±4.5). The number of positive activity peaks also increased from 5±6 (mean±s.d.) in controls to 18±16 and 18±14 in the PefD- and PefDΔSP-expressing lines, respectively. Crucially, lines expressing *cyrA* or *nipA* showed no significant deviation from the baseline (Fig. 6F), identifying PefD as a specific activator of the RIS neuron.

To determine whether this effect is neuron-specific or a general result of heterologous expression, we examined the PVD sensory neuron for neurodegeneration. An indicator for neurodegeneration and neuronal stress are bead-like structures along PVD dendrites (Pop et al., 2024). Although the positive control (*nlp-27*) and PefDΔSP-expressing line showed moderate dendrite degeneration (34% and 34%, respectively), the full-length PefD-expressing line showed no detectable neurodegeneration, similar to the negative control (Fig. S2). This suggests that although intracellular PefD (ΔSP) might have broad effects, the secreted form of the protein specifically modulates RIS-mediated paralysis without inducing general neurotoxicity. Interestingly, the ΔSP variant of PefD, which lacks the signal peptide and is therefore retained intracellularly, still elicited measurable effects. This suggests that PefD can also influence host cells when present intracellularly. However, as this construct is not secreted, these effects likely do not reflect the physiological mode of action of PefD during infection and do not contradict its proposed role as a secreted effector.

DISCUSSION

During infection, nematode-trapping fungi secrete a diverse repertoire of virulence factors and effector proteins to colonize and manipulate their hosts. Although these interactions are central to the predatory lifestyle, the precise molecular mechanisms remain largely elusive (Youssar et al., 2019). Recent transcriptomic and secretomic analyses have highlighted the prominent role of SSPs, which often are strongly induced upon contact with nematodes. PefD – characterized by its length of 72 amino acids, N-terminal signal peptide and stabilizing disulfide bridges – is a hallmark member of this effector class (Kim et al., 2016). Our findings demonstrate that PefD is a critical spatiotemporally regulated virulence factor that facilitates prey immobilization by specifically modulating host neuronal activity.

A central question in the biology of nematode-trapping fungi is whether prey paralysis is a passive byproduct of host stress or an active fungal manipulation. Our virulence assays provide strong evidence for the latter: Δ*pefD* strains exhibited a significantly delayed paralysis time, whereas overexpression accelerated host immobilization.

Heterologous pan-neuronal expression of PefD in *C. elegans* further clarified this role, revealing a robust locomotion phenotype. Worms expressing *pefD*, even without the fungal signal peptide, exhibited significantly reduced speed and travel distances. This

Journal of Cell Science (2026) 139, jcs264962. doi:10.1242/jcs.264962

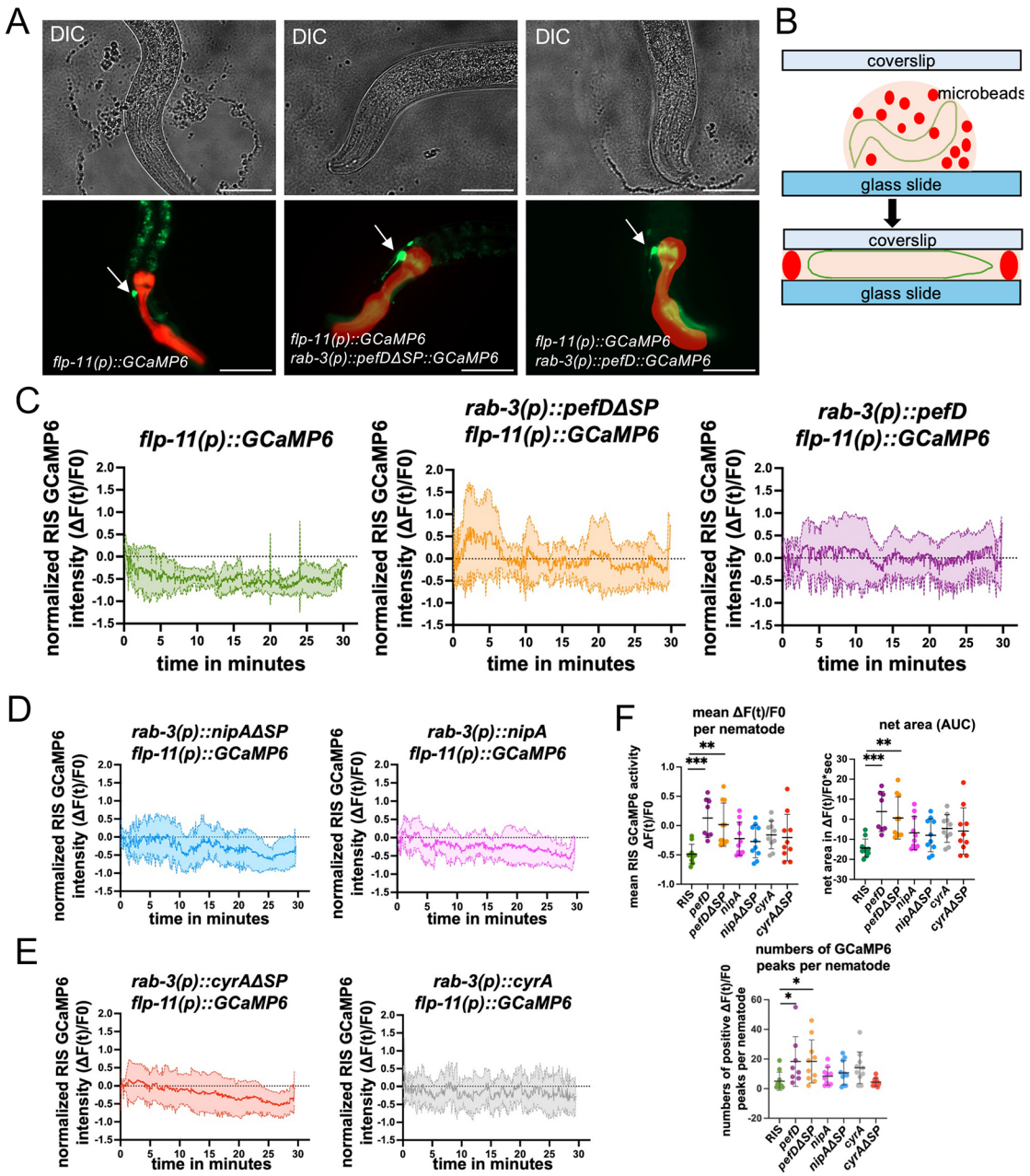


Fig. 6. Neuronal expression of *pefD* enhances overall RIS neuron activity. (A) Representative DIC and fluorescence images of *C. elegans* expressing the Ca^{2+} marker GCaMP6 in the RIS neuron under control of the *flp-11* promoter. Animals expressed either the control construct (*flp-11::GCaMP6*) or additional expression of *pefD* or *pefDΔSP* under the *rab-3* promoter. No difference in the structure of the RIS neuron could be detected. Arrows indicate the RIS neuron. The pharynx is marked with *myo-2(p)::tdTomato*. Scale bars: 50 µm. (B) Scheme of the immobilization setup used for long-term Ca^{2+} imaging. Worms were mounted between a glass slide and a coverslip using a solution of microbeads to restrict movement during imaging. (C–E) Normalized RIS GCaMP6 fluorescence intensity [ΔF(t)/F0] over time. Thick lines show the mean of all the tested animals of one strain. Shaded regions show the variance between individual animals. Dashed lines indicate the null reference point. Only lines expressing *pefD* (C, right) or *pefDΔSP* (C, middle) showed a higher overall activity for the RIS neuron compared to that of the control (C, left). Additional lines expressing *nipA*, *nipAΔSP*, *cyrA* and *cyrAΔSP* are shown for comparison (D,E). (F) Quantification of RIS activity parameters including mean ΔF(t)/F0 per nematode, net activity (area under the curve, AUC) and number of positive GCaMP6 peaks per nematode. Only nematodes expressing *pefD* or *pefDΔSP* under the pan-neuronal *rab-3* promoter showed increased RIS neuron activity compared to the control line *flp-11::GCaMP6*. In contrast, neuronal expression of *nipA* or *cyrA* with or without the signal peptide did not significantly alter RIS activity in comparison to the control. Individual dots represent single animals: control, *n*=10; *pefD*, *n*=8; *pefDΔSP*, *n*=10; *nipA*, *n*=10; *nipAΔSP*, *n*=10; *cyrA*, *n*=10; *cyrAΔSP*, *n*=10. Bars indicate mean±s.d. Statistical significance was determined using a Kruskal–Wallis test with Dunn's post hoc test. **P*≤0.05; ***P*≤0.01; ****P*≤0.005.

effect was far more potent than that observed for CyrA or NipA, suggesting that PefD directly interferes with the neural circuits governing movement. The localization of PefD in host coelomocytes following secretion supports the idea that the protein can navigate the pseudocoelomic space of the host to reach distal targets, potentially even participating in systemic signal transduction through coelomocyte–nerve interactions (Fares and Greenwald, 2001; Gallotta et al., 2020; Park et al., 2010). Although diffusion might contribute to the distribution of PefD within the pseudocoelomic space, it is likely not sufficient to fully explain the rapid onset of

neuronal effects. However, the intensive movements of the trapped nematodes generate connective flows, thereby facilitating more efficient spreading of the protein throughout the body cavity.

The inhibitory effects of PefD appear to be mediated by the RIS interneuron, a key regulator of sleep-like states and locomotion in *C. elegans*. Previous studies in *A. oligospora* showed that RIS activation coincides with the onset of paralysis (Lin et al., 2025). Our Ca^{2+} imaging data confirm that PefD expression significantly increases overall RIS activity, leading to higher GCaMP6 fluorescence and a greater frequency of activation peaks. By acting as a 'stop signal' through RIS, PefD likely triggers the release of inhibitory neurotransmitters such as GABA and neuropeptides such as FLP-11, which suppress motor circuits (Hill et al., 2014; Steuer Costa et al., 2019; Trojanowski and Raizen, 2016). This mechanism bears some phenotypic similarity to *unc-2* or *unc-119* mutants, in which disruptions in Ca^{2+} channels or axonal integrity lead to uncoordinated or slowed movement (Knobel et al., 2001; Maduro and Pilgrim, 1995; Mathews et al., 2003; Schafer and Kenyon, 1995). However, unlike these structural defects, PefD-mediated paralysis is an active, targeted manipulation of the behavioral state of the host.

The structural prediction of PefD via AlphaFold 3 revealed a compact, disulfide-stabilized architecture. Such features are characteristic of many cysteine-rich SSPs found in animal venoms, particularly the inhibitory cystine knot (ICK) peptide family common in spiders and snakes. Although classical ICK peptides typically utilize three disulfide bonds to form their signature 'knot' motif, the two disulfide bonds in PefD likely provide a similar level of exceptional proteolytic and thermal stability within the hostile environment of the host pseudocoel. This structural robustness is often linked to neurotoxic functions. For instance, spider ω-agatoxins target voltage-gated Ca^{2+} channels to block neurotransmitter release, leading to rapid muscular paralysis (Escoubas et al., 2000). Although PefD lacks the full ICK motif, its ability to significantly increase RIS activity suggests that it might function as a fungal 'mini-toxin'. Whether PefD directly modulates ion channels, mimicking the action of venom peptides, or acts through an upstream signaling cascade remains an open question.

To further elucidate the molecular target of PefD, future research should focus on its interaction partners. Yeast two-hybrid screens or pull-down assays could identify specific binding proteins within the *C. elegans* proteome. Furthermore, expressing *pefD* in various Ca^{2+}-channel mutants (e.g. *unc-2*) or conducting transcriptomic profiling of infected nematodes could reveal whether PefD-induced paralysis relies on conserved neurotoxic pathways or a novel fungal mechanism of host manipulation.

MATERIALS AND METHODS

Cultivation of organisms

Arthrobotrys flagrans (strain CBS 349.94) was obtained from the Westerdijk Fungal Biodiversity Institute culture collection (Utrecht, the Netherlands). Fungal cultures were maintained on PDA plates and incubated at 28°C. The *Caenorhabditis elegans* WT strain N2 and all derivative transgenic lines were maintained on nematode growth medium (NGM) plates seeded with *Escherichia coli* OP50. Cultivation, handling and synchronization of nematode populations were performed according to standard protocols described in the WormBook (Stiernagle, 2006).

Generation of transgenic organisms

Protoplast-mediated transformation *of A. flagrans* was performed as previously described (Emser et al., 2025). Briefly, 6×10^6 protoplasts were incubated with 7 µg of donor DNA. Transformants were selected on PDA plates supplemented with the appropriate antibiotics: hygromycin B (100 µg/ml), geneticin (G418) (150 µg/ml) or nourseothricin (100 µg/ml). Following incubation at 28°C for 4–7 days, resistant colonies were isolated for further molecular verification. Multiple independent transformants were initially obtained. For further analyses, a representative transformant was selected.

To generate transgenic *C. elegans* lines carrying extrachromosomal arrays, plasmid DNA was microinjected into the gonad arms of young adult hermaphrodites. This results in the formation of extrachromosomal arrays that are maintained episomally and are not integrated into the genome. These arrays are inherited in a mosaic manner and were identified by the co-expression of the fluorescent marker in the pharynx of the F_1 progeny. The injection mix contained the *pefD* fusion construct (5 ng/µl), a pharyngeal co-injection marker (5 ng/µl) of either *myo-2(p)::tdTomato* or *myo-2(p)::GFP*, and 140 ng/µl of a 1 kb DNA ladder (New England Biolabs) as carrier DNA to reach a final concentration of 150 ng/ µl.

All organisms used in this study are listed in Table S1.

Plasmid constructions

All plasmids are listed in Table S2 and the used oligonucleotides in Table S3. For the ABTS-assay, the modified vector pOF018 was used for the expression of the *A. nidulans lccC* gene (NCBI XP_663001.1) under the constitutive *A. nidulans* glyceraldehyde-3-phosphate dehydrogenase (*gpdA*) promoter as described (Youssar et al., 2019). The *pefD* fusion plasmid for the ABTS assay and the control plasmid were constructed using the Gibson assembly method. The *pefD* gene sequence was fused to the 3′ end of the laccase C gene in the vector backbone. Standard protocols were used for *E. coli* transformation and plasmid isolation (Green and Sambrook, 2012; Sambrook and Russell, 1999). For the promoter fusion, 1.5 kb upstream of the *pefD* ORF was amplified from gDNA with overhangs and cloned in the pVW23 vector. The vector was amplified using primers that bind outside the *h2B* promoter. Both amplicons were assembled in a 3:1 ratio using Gibson assembly.

Plasmids for PefD localization were constructed with the Gibson assembly method. For the C-terminal GFP fusion to DFL_005559 (*pefD*) without the signal peptide, the gene was amplified with a forward primer starting at 85 bp with a start codon and overlap in the backbone and a reverse primer containing an overlap in the GFP. The amplicon was inserted in the vector pJM08.

For the C-terminal GFP fusion to DFL_005559 (*pefD*) with the native promoter, the gene was amplified with its promoter from genomic DNA (gDNA) and inserted in the vector pNH32. For the C-terminal mCherry fusion to *pefD* with its native promoter, the gene with its promoter were cloned in the vector pJM16. For the C-terminal GFP fusion to only the signal peptide from *pefD*, the first 84 bp were amplified and cloned into the vector pJM08.

The *pefD* gene was deleted by homologous recombination. 1.5 kb flanks homologous to the 5′ and 3′ regions of the *pefD* gene were amplified by PCR, using *A. flagrans* gDNA as template. The hygromycin B resistance cassette *hph* was amplified using pFC332 as template (Nodvig et al., 2015). The PCR fragments were assembled into the pJET1.2 vector (Thermo Fisher Scientific). To reintroduce the functional *A. flagrans pefD* gene into the *pefD* deletion strain, the whole *pefD* gene, including its 1.5 kb upstream and 1.5 kb downstream regulatory regions, was amplified via PCR, using *A. flagrans* gDNA as template. To select for transformants, the geneticin G418 resistance cassette was used. In a cloning step, the G418 resistance cassette was assembled between the *trpC* promoter and *trpC* terminator fragment of pVW23 using Gibson assembly. Lastly, the new G418 resistance cassette and the *pefD* complement were assembled into the pJET1.2 vector.

For heterologous expression of *pefD* in *C. elegans*, the ORF was amplified with or without the signal peptide (aa 1–28) from cDNA and cloned in a modified version of the pPF37 vector using Gibson assembly. For the localization of PefD inside the nematode, *pefD* was tagged C-terminally with mScarlet. The construct was expressed under the pan-tissue *eft-3* promoter. For pan-neuronal expression, *pefD* was expressed under the *rab-3* promoter.

ABTS assay

ABTS assay was performed as described previously (Wernet et al., 2021; Youssar et al., 2019). *A. flagrans* transformants were inoculated on PDA

Journal of Cell Science (2026) 139, jcs264962. doi:10.1242/jcs.264962

plates with 1 mM ABTS (Merck) with a toothpick and incubated for 48 h at 28°C. Laccase activity was correlated with the formation of the blue-green ABTS radical.

Trap induction

To induce trap formation, spores of *A. flagrans* were inoculated on thin low-nutrient agar (LNA) slides (1 g/l KCl, 0.2 g/l $MgSO_4{\cdot}7H_2O$, 0.4 mg/l $MnSO_4{\cdot}4H_2O$, 0.88 mg/l $ZnSO_4{\cdot}7H_2O$, 3 mg/l $FeCl_3{\cdot}6H_2O$, 15 g/l agar, pH 6) and co-incubated with *C. elegans* at 28°C in the dark for 24 h.

RNA extraction and qRT-PCR

To induce traps for RNA extraction, 10^6 *A. flagrans* spores were incubated on LNA plates covered with a cellophane membrane for 24 h at 28°C. A mixed *C. elegans* population was added to the membrane and co-incubated for 24 h to induce trap formation. The uninduced samples were grown without nematodes for 48 h at 28°C.

For RNA extraction, the mycelium was scratched off the cellophane membrane and ground in liquid N_2. Total RNA was extracted with TRIzol reagent (Invitrogen). DNase digestion was performed using the Turbo DNA-free Kit (Invitrogen) and the RNA was diluted to 50 ng/µl. The Luna Universal One-Step RT-qPCR Kit (New England Biolabs) was used for qRT-PCR analysis on a CFX Connect Real-Time PCR Detection System (Bio-Rad). Each reaction mixture contained 0.2 µM primers and 100 ng of RNA in a 20 µl total volume. The γ-actin orthologue DFL_002353 was used as an internal reference gene for normalization. The qRT-PCR was performed using three biological replicates. Significance was calculated using an unpaired two-tailed Student's *t*-test. Significance was considered as follows: ns, not significant, $P>0.05$; *$P\leq0.05$; **$P\leq0.01$; ***$P\leq0.005$; ****$P\leq0.0001$.

Southern hybridization

To verify *pefD* deletion, Southern blot analysis was conducted. gDNA from mutants and WT strains was isolated and digested overnight with the respective restriction enzymes (New England Biolabs). The analysis followed standard protocols. A labeling probe was generated by PCR amplification of 1 kb of the *pefD* 3′ flanking site using digoxigenin-labeled dNTPs (Roche) and specific primers. The DNA was transferred to a nylon membrane (Roti-Nylon plus, Roth, Karlsruhe, Germany) and incubated overnight with a 1:10,000 dilution of anti-digoxigenin-AP fab Fragment (11093274910, Roche). For development of the membrane, CDP-Star solution (Roche) was added right before the exposure in a Chemi-Smart chemiluminescence system (Amersham ImageQuant 800, Cytiva).

Virulence assay

To investigate the effect of *pefD* deletion on the virulence of *A. flagrans*, a virulence assay was conducted. Spores of the designated strains were transferred to thin LNA slides. To induce trap formation, the fungus was co-incubated with a mixed population of *C. elegans*. After 24 h, trap formation was checked under the microscope. Non-captured nematodes were washed off with dH_2O from the slides and areas with many traps were marked and transferred into an ibidi chamber. Long-term recordings were made using a Zeiss Axio Observer.Z1 microscope equipped with a multi-laser module, a spinning disk module (CSU-X1M 5000) and an AxioCam MRm camera. Multiple positions with traps were saved and a synchronized population of L4 WT nematodes was added just before the start of the recording. The experiment was set to run for 11 h, capturing images approximately every 11 min in the differential interference contrast (DIC) channel per position. Recordings were analyzed for paralysis time. Due to the multi-position imaging setup, individual animals were not recorded continuously. The paralysis time was measured as the interval between the first contact of the nematode with the trap until it did not move anymore. The experiments were repeated in biological and technical replicates. The statistical significance was calculated using an unpaired two-tailed Student's *t*-test. Significance was considered as follows: ns, not significant, $P>0.05$; *$P\leq0.05$; **$P\leq0.01$; ***$P\leq0.005$; ****$P\leq0.0001$.

Ca^{2+} imaging in RIS neurons

To check for RIS activity in *C. elegans*, GCaMP6 was expressed under the *flp-11* promoter. GCaMP6 is a genetically encoded Ca^{2+} indicator composed of a circularly permuted GFP fused to calmodulin and the M13 peptide. Upon binding of Ca^{2+}, calmodulin undergoes a conformational change that promotes interaction with M13, resulting in increased fluorescence of the GFP chromophore. Thus, changes in fluorescence intensity serve as a proxy for intracellular Ca^{2+} levels and neuronal activity. Designated nematodes were transferred on thin 3% agarose slides and immobilized with a solution of polystyrene beads (0.1 µm; Merck) and a coverslip. Recordings were made for 30 min, capturing images each 5 s in the GFP channel. Analyses were done in Fiji (Schindelin et al., 2012) by measuring the fluorescence intensity of GCaMP6 of the RIS neuron cell body. The fluorescence intensity was normalized against the baseline, which is the average fluorescence intensity of the first minute. Data were calculated as (fluorescence intensity at each frame – baseline)/baseline [(F(t)−F0)/F0]. For statistics, the mean fluorescence of GCaMP6 of single worms, the net area and the number of positive peaks were measured and compared. Statistical analysis was performed using the Kruskal–Wallis test followed by Dunn's multiple comparison post hoc test to compare group differences. All analyses were conducted in GraphPad Prism (version 10.5.0). Significance was considered as follows: ns, not significant, $P>0.05$; *$P\leq0.05$; **$P\leq0.01$; ***$P\leq0.005$; ****$P\leq0.0001$.

Movement analysis of *C. elegans*

To analyze the movement of *C. elegans*, recordings were made for 1 min capturing images each second in the DIC channel. Analyses were done by Fiji by manually tracking the nematode and measuring the speed and total distance travelled. Statistical analysis was performed using the Kruskal–Wallis test followed by Dunn's multiple comparison post hoc test to compare group differences. All analyses were conducted in GraphPad Prism (version 10.5.0). Significance was considered as follows: ns, not significant, $P>0.05$; *$P\leq0.05$; **$P\leq0.01$; ***$P\leq0.005$; ****$P\leq0.0001$.

Quantification of PVD dendrite neurodegeneration in *C. elegans*

To quantify neurodegeneration in the PVD dendrites, the nematodes were picked on thin 3% LNA pads and 20 mM NaN_3 was used to inhibit movement. The degeneration was characterized as bead-like structures along the PVD dendrites. These structures were counted at 40× magnification. Nematodes with a total of ten or more of these bead-like structures in more than five menorahs of the PVD dendrites were considered to have neurodegeneration. This quantification was reported as a percentage.

Microscopy

For microscopy, spores were inoculated on thin LNA slides using a sterile toothpick and incubated for at least 24 h at 28°C with a mixed population of *C. elegans* to induce trap formation. Conventional fluorescence images were captured at room temperature using a Zeiss Plan-Apochromat 63×/1.4 oil DIC, EC Plan-Neofluar 40×/0.75, EC Plan-Neofluar 20×/0.50 or EC Plan-Neofluar 10×/0.30 objective attached to a Zeiss AxioImager Z.1 and AxioCamMR. Color images were acquired using the AxioCam 105 color. Images were collected using ZEN 2012 Blue Edition software. For work with *C. elegans*, a Zeiss SteREO Discovery.V12 and a Zeiss SteREO Lumar.V1 with fluorescence filters were used. For long-term recordings, a Zeiss AxioObserver.Z1 equipped with a Zeiss multi-laser module (488 nm diode laser and 561 nm OPSL laser), a spinning disk module CSU-X1M 5000 and an AxioCam MRm was used.

Acknowledgements

X.H. was a fellow of the Chinese Scholar Council (CSC).

Competing interests

The authors declare no competing or financial interests.

Author contributions

Conceptualization: R.F.; Data curation: A.-L.K.; Formal analysis: A.-L.K.; Funding acquisition: R.F.; Investigation: A.-L.K., X.H., P.S.; Methodology: A.-L.K., X.H., P.S., E.W.; Project administration: R.F.; Supervision: N.W., V.W., R.F.; Validation: R.F.; Visualization: A.-L.K., R.F.; Writing – original draft: A.-L.K.; Writing – review & editing: R.F.

Funding

This work was funded by the Deutsche Forschungsgemeinschaft (Fi 459/27-1 and Fi 459/26-1).

Data and resource availability

All relevant data and details of resources can be found within the article and its supplementary information.

References

Abramson, J., Adler, J., Dunger, J., Evans, R., Green, T., Pritzel, A., Ronneberger, O., Willmore, L., Ballard, A. J., Bambrick, J. et al. (2024). Accurate structure prediction of biomolecular interactions with AlphaFold 3. *Nature* **630**, 493-500. doi:10.1038/s41586-024-07487-w

Emser, J., Wernet, N., Hetzer, B., Wohlmann, E. and Fischer, R. (2024). The small cysteine-rich virulence factor NipA of *Arthrobotrys flagrans* interferes with cuticle integrity of *Caenorhabditis elegans*. *Nat. Commun.* **15**, 5795. doi:10.1038/s41467-024-50096-4

Emser, J., Seidler, L., Kovacevic, E., Yu, K., Rudolf, T., Wohlmann, E. and Fischer, R. (2025). The Egh16-like virulence factor TrsA of the nematode-trapping fungus *Arthrobotrys flagrans* facilitates intrusion into its host *Caenorhabditis elegans*. *PLoS Pathog.* **21**, e1013370. doi:10.1371/journal.ppat.1013370

Escoubas, P., Diochot, S. and Corzo, G. (2000). Structure and pharmacology of spider venom neurotoxins. *Biochimie* **82**, 893-907. doi:10.1016/S0300-9084(00)01166-4

Fan, Y., Du, M., Zhang, W., Deng, W., Yang, E., Wang, S., Yan, L., Zhang, L., Kang, S., Steenwyk, J. L. et al. (2025). The genomes of nematode-trapping fungi provide insights into the origin and diversification of fungal carnivorism. *Mol. Phylogenet. Evol.* **212**, 108423. doi:10.1016/j.ympev.2025.108423

Fares, H. and Greenwald, I. (2001). Genetic analysis of endocytosis in *Caenorhabditis elegans*: coelomocyte uptake defective mutants. *Genetics* **159**, 133-145. doi:10.1093/genetics/159.1.133

Fischer, R. and Requena, N. (2022). Small secreted proteins as virulence factors in nematode-trapping fungi. *Trends Microbiol.* **30**, 616-617. doi:10.1016/j.tim.2022.03.005

Gallotta, I., Sandhu, A., Peters, M., Haslbeck, M., Jung, R., Agilkaya, S., Blersch, J. L., Rodelsperger, C., Roseler, W., Huang, C. et al. (2020). Extracellular proteostasis prevents aggregation during pathogenic attack. *Nature* **584**, 410-414. doi:10.1038/s41586-020-2461-z

Gomez, M. V., Kalapothakis, E., Guatimosim, C. and Prado, M. A. (2002). Phoneutria nigriventer venom: a cocktail of toxins that affect ion channels. *Cell. Mol. Neurobiol.* **22**, 579-588. doi:10.1023/A:1021836403433

Green, M. R. and Sambrook, J. (2012). *Molecular cloning: A laboratory manual* (4th edition), Cold Spring Harbor Laboratory Press, Cold Spring Harbor, New York.

Gundersen, C. B., Jenden, D. J. and Newton, M. W. (1981). Beta-bungarotoxin stimulates the synthesis and accumulation of acetylcholine in rat phrenic nerve diaphragm preparations. *J. Physiol.* **310**, 13-35. doi:10.1113/jphysiol.1981.sp013535

Hill, A. J., Mansfield, R., Lopez, J. M., Raizen, D. M. and Van Buskirk, C. (2014). Cellular stress induces a protective sleep-like state in *C. elegans*. *Curr. Biol.* **24**, 2399-2405. doi:10.1016/j.cub.2014.08.040

Hood, H. M., Neafsey, D. E., Galagan, J. and Sachs, M. S. (2009). Evolutionary roles of upstream open reading frames in mediating gene regulation in fungi. *Annu. Rev. Microbiol.* **63**, 385-409. doi:10.1146/annurev.micro.62.081307.162835

Hsueh, Y. P., Mahanti, P., Schroeder, F. C. and Sternberg, P. W. (2013). Nematode-trapping fungi eavesdrop on nematode pheromones. *Curr. Biol.* **23**, 83-86. doi:10.1016/j.cub.2012.11.035

Hsueh, Y. P., Gronquist, M. R., Schwarz, E. M., Nath, R. D., Lee, C. H., Gharib, S., Schroeder, F. C. and Sternberg, P. W. (2017). Nematophagous fungus *Arthrobotrys oligospora* mimics olfactory cues of sex and food to lure its nematode prey. *eLife* **6**, e20023. doi:10.7554/eLife.20023

Hu, X., Hoffmann, D., Wang, M., Schuhmacher, L., Stroe, M. C., Schreckenberger, B., Elstner, M. and Fischer, R. (2024). GprC of the nematode-trapping fungus *Arthrobotrys flagrans* activates mitochondria and reprograms fungal cells for nematode hunting. *Nat. Microbiol.* **9**, 1752-1763. doi:10.1038/s41564-024-01731-9

Jiang, X., Xiang, M. and Liu, X. (2017). Nematode-trapping fungi. *Microbiol. Spectr.* **5**, FUNK-0022. doi:10.1128/microbiolspec.FUNK-0022-2016

Kim, K. T., Jeon, J., Choi, J., Cheong, K., Song, H., Choi, G., Kang, S. and Lee, Y. H. (2016). Kingdom-wide analysis of fungal small secreted proteins (SSPs) reveals their potential role in host association. *Front. Plant Sci.* **7**, 186. doi:10.3389/fpls.2016.00186

Knobel, K. M., Davis, W. S., Jorgensen, E. M. and Bastiani, M. J. (2001). UNC-119 suppresses axon branching in *C. elegans*. *Development* **128**, 4079-4092. doi:10.1242/dev.128.20.4079

Kriegler, M., Wernet, V., Hetzer, B., Herrero, S., Wei, A., Wäckerle, J., Dewein, I. and Fischer, R. (2025). Cell-end marker proteins are required for hyphal ring formation and size determination of traps of *Arthrobotrys flagrans*. *J. Cell Sci.* **138**, jcs263744. doi:10.1242/jcs.263744

Kuo, C. Y., Tay, R. J., Lin, H. C., Juan, S. C., Vidal-Diez de Ulzurrun, G., Chang, Y. C., Hoki, J., Schroeder, F. C. and Hsueh, Y. P. (2024). The nematode-trapping fungus *Arthrobotrys oligospora* detects prey pheromones via G protein-coupled receptors. *Nat. Microbiol.* **9**, 1738-1751. doi:10.1038/s41564-024-01679-w

Lin, H. C., de Ulzurrun, G. V., Chen, S. A., Yang, C. T., Tay, R. J., Iizuka, T., Huang, T. Y., Kuo, C. Y., Goncalves, A. P., Lin, S. Y. et al. (2023). Key processes required for the different stages of fungal carnivory by a nematode-trapping fungus. *PLoS Biol.* **21**, e3002400. doi:10.1371/journal.pbio.3002400

Lin, T. H., Chang, H. W., Tay, R. J. and Hsueh, Y. P. (2025). Predation by nematode-trapping fungus triggers mechanosensory-dependent quiescence in *Caenorhabditis elegans*. *iScience* **28**, 112792. doi:10.1016/j.isci.2025.112792

Maduro, M. and Pilgrim, D. (1995). Identification and cloning of unc-119, a gene expressed in the *Caenorhabditis elegans* nervous system. *Genetics* **141**, 977-988. doi:10.1093/genetics/141.3.977

Mathews, E. A., Garcia, E., Santi, C. M., Mullen, G. P., Thacker, C., Moerman, D. G. and Snutch, T. P. (2003). Critical residues of the *Caenorhabditis elegans unc-2* voltage-gated calcium channel that affect behavioral and physiological properties. *J. Neurosci.* **23**, 6537-6545. doi:10.1523/JNEUROSCI.23-16-06537.2003

Nodvig, C. S., Nielsen, J. B., Kogle, M. E. and Mortensen, U. H. (2015). A CRISPR-Cas9 system for genetic engineering of filamentous fungi. *PLoS ONE* **10**, e0133085. doi:10.1371/journal.pone.0133085

Park, S. K., Link, C. D. and Johnson, T. E. (2010). Life-span extension by dietary restriction is mediated by NLP-7 signaling and coelomocyte endocytosis in *C. elegans*. *FASEB J.* **24**, 383-392. doi:10.1096/fj.09-142984

Pop, M., Klemke, A. L., Seidler, L., Wernet, N., Steudel, P. L., Baust, V., Wohlmann, E. and Fischer, R. (2024). Caenorhabditis elegans neuropeptide NLP-27 enhances neurodegeneration and paralysis in an opioid-like manner during fungal infection. *iScience* **27**, 109484. doi:10.1016/j.isci.2024.109484

Ranawaka, U. K., Lalloo, D. G. and de Silva, H. J. (2013). Neurotoxicity in snakebite–the limits of our knowledge. *PLoS Negl. Trop. Dis.* **7**, e2302. doi:10.1371/journal.pntd.0002302

Sambrook, J., and Russell, D. W. (1999). *Molecular Cloning: A Laboratory Manual*. Cold Spring Harbor, New York: Cold Spring Harbor Laboratory Press.

Schafer, W. R. and Kenyon, C. J. (1995). A calcium-channel homologue required for adaptation to dopamine and serotonin in *Caenorhabditis elegans*. *Nature* **375**, 73-78. doi:10.1038/375073a0

Schindelin, J., Arganda-Carreras, I., Frise, E., Kaynig, V., Longair, M., Pietzsch, T., Preibisch, S., Rueden, C., Saalfeld, S., Schmid, B. et al. (2012). Fiji: an open-source platform for biological-image analysis. *Nat. Methods* **9**, 676-682. doi:10.1038/nmeth.2019

Sperschneider, J., Dodds, P. N., Gardiner, D. M., Singh, K. B. and Taylor, J. M. (2018). Improved prediction of fungal effector proteins from secretomes with EffectorP 2.0. *Mol. Plant Pathol.* **19**, 2094-2110. doi:10.1111/mpp.12682

Steuer Costa, W., Van der Auwera, P., Glock, C., Liewald, J. F., Bach, M., Schuler, C., Wabnig, S., Oranth, A., Masurat, F., Bringmann, H. et al. (2019). A GABAergic and peptidergic sleep neuron as a locomotion stop neuron with compartmentalized Ca^{2+} dynamics. *Nat. Commun.* **10**, 4095. doi:10.1038/s41467-019-12098-5

Stiernagle, T. (2006). Maintenance of *C. elegans*. In *WormBook*, (ed. The *C. elegans* Research Community). doi:10.1895/wormbook.1.101.1

Tasoulis, T. and Isbister, G. K. (2017). A review and database of snake venom proteomes. *Toxins (Basel)* **9**, 290. doi:10.3390/toxins9090290

Trojanowski, N. F. and Raizen, D. M. (2016). Call it worm sleep. *Trends Neurosci.* **39**, 54-62. doi:10.1016/j.tins.2015.12.005

Turek, M., Lewandrowski, I. and Bringmann, H. (2013). An AP2 transcription factor is required for a sleep-active neuron to induce sleep-like quiescence in *C. elegans*. *Curr. Biol.* **23**, 2215-2223. doi:10.1016/j.cub.2013.09.028

Vidal-Diez de Ulzurrun, G. and Hsueh, Y. P. (2018). Predator-prey interactions of nematode-trapping fungi and nematodes: both sides of the coin. *Appl. Microbiol. Biotechnol.* **102**, 3939-3949. doi:10.1007/s00253-018-8897-5

Wernet, N., Wernet, V. and Fischer, R. (2021). The small-secreted cysteine-rich protein CyrA is a virulence factor of *Duddingtonia flagrans* during the *Caenorhabditis elegans* attack. *PLoS Pathog.* **17**, e1010028. doi:10.1371/journal.ppat.1010028

Wernet, V., Kriegler, M., Kumpost, V., Mikut, R., Hilbert, L. and Fischer, R. (2023). Synchronization of oscillatory growth prepares fungal hyphae for fusion. *eLife* **12**, e83310. doi:10.7554/eLife.83310

Wernet, V., Wäckerle, J. and Fischer, R. (2022). The STRIPAK component SipC is involved in morphology and cell-fate determination in the nematode-trapping fungus *Duddingtonia flagrans*. *Genetics* **220**, iyab153. doi:10.1093/genetics/iyab153

Youssar, L., Wernet, V., Hensel, N., Yu, X., Hildebrand, H.-G., Schreckenberger, B., Kriegler, M., Hetzer, B., Frankino, P., Dillin, A. et al. (2019). Intercellular communication is required for trap formation in the nematode-trapping fungus *Duddingtonia flagrans*. *PLoS Genet.* **15**, e1008029. doi:10.1371/journal.pgen.1008029

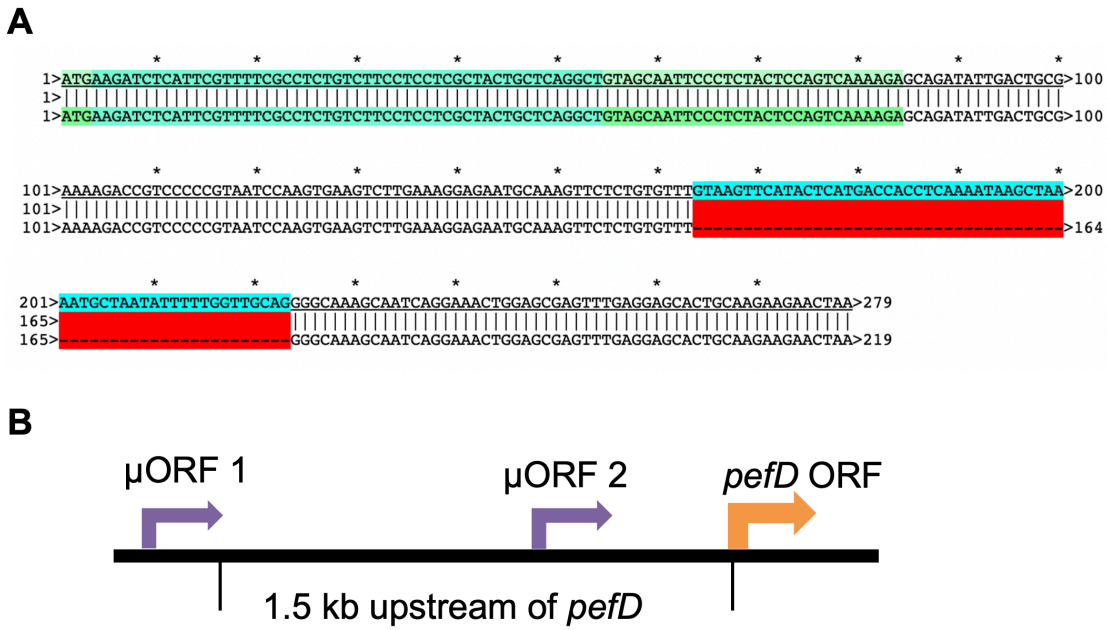


Fig. S1. Scheme of the *pefD* locus. (A) Genomic DNA (top) and spliced mRNAs sequence (bottom). The predicted N-terminal signal peptide is highlighted in green. The intron, as deduced from RNAseq data, is indicated in blue and red. The intron spans 60 nucleotides corresponding to codons 55-75 within the *pefD*-open reading frame. **(B)** Scheme of the 1.5 kb upstream region of *pefD* with two putative μORFs.

Journal of Cell Science • Supplementary information

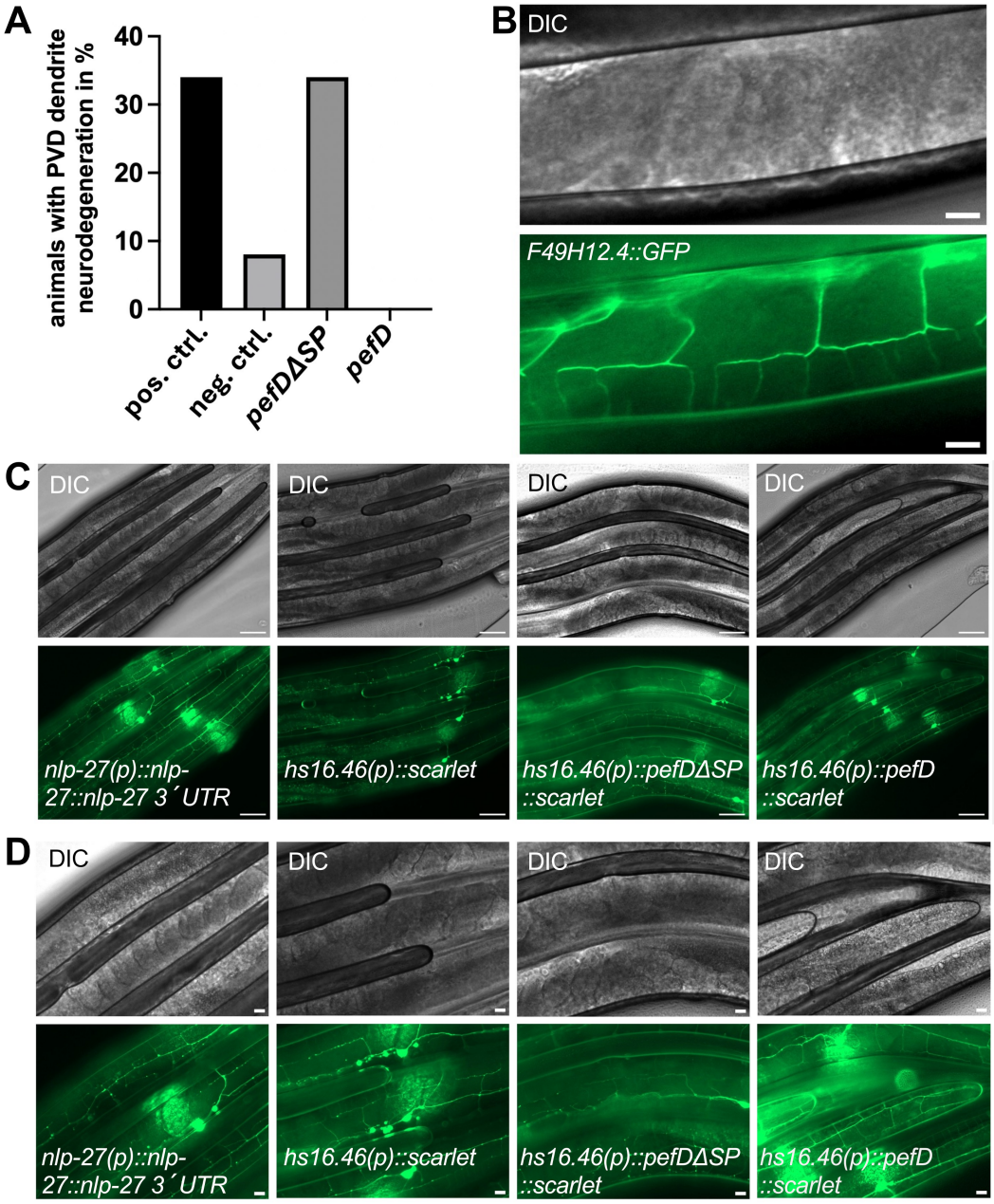


Fig. S2. Analysis of PVD neuron morphology after heterologous expression of *pefD*. (A) Quantification of PVD dendrite degeneration in the analyzed *C. elegans* lines. The fraction of animals displaying dendritic degeneration is shown for the positive control (*nlp-27(p)::nlp-27::nlp-27 3´UTR*), the negative control (*hsp-16.48(p)::scarlet*), and lines expressing *pefD::scarlet* or *pefDΔSP::scarlet* under the heat-shock promotor *hsp-16.48* promotor. **(B)** Representative fluorescence image of the PVD neuron in strain NC1686 expressing GFP in the PVD neuron, showing normal dendritic morphology without signs of degeneration **(C)** Representative fluorescence images of worms from the tested lines. PVD dendrite degeneration is characterized by the appearance of bead-like structures along the dendrites. **(D)** Magnified views of regions shown in C. Scale bar 10 μm for all panels.

Journal of Cell Science • Supplementary information

Table S1. strains used in this study.

Strain	Genotype	Reference
A. flagrans		
Wildtyp		CBS-KNAW Westerdijk Fungal Biodiversity Institute (Utrecht, NL)
sAK15	*gpdA(p)::pefD::LccCΔSP* pXD19	This work
sAK17	*gpdA(p)::pefDΔSP::LccCΔSP* pAK55	This work
sAK18	sXD35 x *pefD(p)::pefD::pefD(t)* pAK74	This work
sAK19	sVW10 x *pefD(p)::h2B::mCherry* pXD17	This work
sAK21	*pefD(p)::pefD::mCherry* pXD41	This work
sAK23	sXD35 x *pefD(p)::pefD::GFP* pAK65	This work
sAK25	*oliC(p)::SP(pefD)::GFP::gluc(t)* pAK67	This work
sAK26	*oliC(p)::pefDΔSP::GFP::gluc(t)* pAK68	This work
sVW10	*h2b(p)::h2b::GFP* pJW04	(Wernet et al., 2022)
sXD26	*pefD(p)::pefD::GFP* pXD32	This work
sXD28	sNH30 x *pefD(p)::pefD::mCherry* pXD41	This work
sXD30	sXD26 x *nipA(p)::nipA::mCherry* pJM16	This work
sXD33	*olic(p)::pefD::gluc(t) pXD52*	This work
sXD35	*ΔpefD* pXD42	This work
C. elegans		
N2		University of Freiburg
CeAK16	N2 x *eft-3(p)::pefD::wrmScarlet::unc-54 3`UTR* pAK42	This work
CeAK17	N2 x *rab-3(p)::pefD::unc-54 3`UTR* pAK62	This work
CeAK18	N2 x *rab-3(p)::pefDΔSP::unc-54 3`UTR* pAK63	This work
CeAK21	N2 RIS x *rab-3(p)::cyrA::unc-54 3`UTR* pAK80	This work

CeAK22	N2 RIS x *rab-3(p)::nipAΔSP::unc-54 3`UTR* pAK77	This work
CeAK23	N2 RIS x *rab-3(p)::nipA::unc-54 3`UTR* pAK78	This work
CeAK24	N2 RIS x *rab-3(p)::cyrAΔSP::unc-54 3`UTR* pAK79	This work
CeAK25	N2 x *hsp-16.46(p)::pefD::wrmScarlet::unc-54 3`UTR* pAK60	This work
CeAK26	N2 x *hsp-16.46(p):: pefDΔSP::wrmScarlet::unc-54 3`UTR* pAK57	This work
CeAK28	*N2 x eft-3(p)::pefDΔSP::wrmScarlet::unc-54 3`UTR* pAK56	This work
CeAK30	N2 RIS x *rab-3(p)::pefD::unc-54 3`UTR* pAK62	This work
CeAK31	N2 RIS x *rab-3(p)::pefDΔSP::unc-54 3`UTR* pAK63	This work
CeAK32	NC1686 x *hsp-16.46(p)::pefD::wrmScarlet::unc-54 3`UTR* pAK60	This work
CeAK33	NC1686 x *hsp-16.46(p)::pefDΔSP::wrmScarlet::unc-54 3`UTR* pAK57	This work
CeAK34	NC1686 x *hsp-16.46(p)::wrmScarlet::unc-54 3`UTR* pNH59	This work
NC1686	wdIs51 F49H12.4::GFP + unc-119(+)	CGC
N2 RIS	N2 x *flp-11::GCamP6* pPS01	P. Steudel
KIT27	*rfl3 [NC1686 + nlp-27(p)::nlp-27::nlp-27 3' UTR + myo-2(p)::dTtomato*]	(Pop et al., 2024)
E. coli		
Top10	F− *mcrA* _(*mrr-hsdRMSmcrBC*)_80*lacZ_M15* _*lacX74 recA1 araD139* _(*ara-leu)7697 galU galK rpsL* (StrR) *endA1* nupG	Invitrogen (Karlsruhe)
OP50	ura-	University of Freiburg

Table S2. Plasmids used in this study.

Name	Description	Reference
pAK42	*eft-3(p)::pefD::wrmScarlet::unc-54 3`UTR*	This work
pAK55	*gpdA(p)::pefDΔSP::LccCΔSP*	This work
pAK57	*hsp-16.46(p)::pefDΔSP::wrmScarlet::unc-54 3`UTR*	This work
pAK60	*hsp-16.46(p)::pefD::wrmScarlet::unc-54 3`UTR*	This work
pAK62	*rab-3(p)::pefD::unc-54 3`UTR*	This work
pAK63	*rab-3(p)::pefDΔSP::unc-54 3`UTR*	This work
pAK65	*pefD(p)::pefD::GFP;* nat	This work
pAK67	*oliC(p)::SP(pefD)::GFP::tgluc; trpC(p)::hph::trpC(t) (hph)*	This work
pAK68	*oliC(p)::pefDΔSP::gfp::tgluc; hph*	This work
pAK77	*rab-3(p)::nipAΔSP::unc-54 3`UTR*	This work
pAK78	*rab-3(p)::nipA::unc-54 3`UTR*	This work
pAK79	*rab-3(p)::cyrAΔSP::unc-54 3`UTR*	This work
pAK80	*rab-3(p)::cyrA::unc-54 3`UTR*	This work
pNH32	*cyrA(p)::cyrA::GFP::gluC(t); hph*	[3]
pNH59	*hsp-16.48(p)::wrmScarlet::unc-54 3´UTR*	[3]
pJM08	*oliC(p)::nipA::gfp::gluC(t); hph*	[4]
pJM16	*nipA(p)::nipA::mCherry::gluC(t); g418*	[4]

Journal of Cell Science • Supplementary information

pXD17	*pefD(p)::h2B::mCherry::Ttub; hph*	This work
pXD19	*gpdA(p)::pefD::LccCΔSP; hph*	This work
pXD32	*pefD(p)::pefD::GFP; hph*	This work
pXD41	*pefD(p)::pefD::GFP; gpdA(p)::g418::trpC(t) (g418)*	This work
pXD42	*pefD(LB)::hph::pefD(RB)*	This work
pXD52	*olic(p)::pefD::gluc(t); hph*	This work
pXD74	*pefD(p)::pefD::pefD(t); g418*	This work
pCFJ90T	*myo-2(p)::tdTomato*	A. Dillin, UC Berkeley
pMyo-2-EGFP	*myo-2(p)::GFP*	R. Baumeister, Uni. Freiburg
pOF018	*gpdA(p)::lccC; hph; Pyr4*	Oleksandra Fokina, Karlsruhe
pVW23	*h2B(p)::h2B::mCherry::h2B(t); hph*	Valentin Wernet, Karlsruhe
pFC332	*AMA1, tef1(p)::Cas9::tef1(t); hph*	Uffe H. Mortensen (Technical University of Denmark, Lyngby)
pPF37	*ttTi5605 cb-unc-119 (based on pCFJ350)*	Phil Frankino, UC Berkeley

Journal of Cell Science • Supplementary information

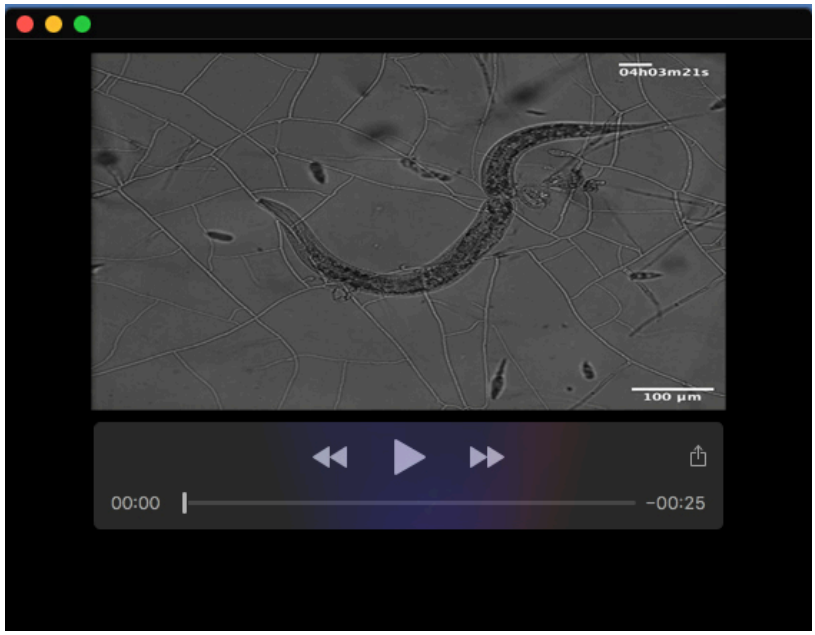
Table S3. Oligonucleotides used in this study.

Name	Sequence (from 5' to 3')	Description
5559_gpd_for	CAGGCGCGCCATGAAGATCTCATTCGTTTTCG	PefD/Laccase fusion with SP
5559_LA_rev	GAACCGGTGTTCTTCTTGCAGTGCTCCT	PefD/Laccase fusion with SP
OL_pefDohneSP28_fwd	TGAGCAGACATCACAGGCGCGCCATGGCAGATATTGACTGCGAAAAGAC	PefD/Laccase fusion without SP
PefD_OL_Lacc_rev	GTCGTGCTCAAAGACCCAAGAACCGGTGTTCTTCTTGCAGTGCTCCTC	PefD/Laccase fusion without SP
P5559_h2b_ol_for	TTGTAAAACGACGGCCAGTGAATTCCGAAGACCTTTGCTGTTCTC	PefD/mCherry promoter fusion
P5559_h2b_ol_rev	TCGGCGGCGGCTTTTGGTGGCATTTTGATAGTATGAAAGTTTATATGGTT	PefD/mCherry promoter fusion
df_h2b_fwd	ATGCCACCAAAAGCCGCC	PefD/mCherry promoter fusion
pJM10_rev	GAATTCACTGGCCGTCGTTT	PefD/mCherry promoter fusion
5559_RT_for	ATGAAGATCTCATTCGTTTTCGC	qRT-PCR
5559_RT_rev	TAGTTCTTCTTGCAGTGCTCC	qRT-PCR
qpcr_hk_actin2_fwd	TCCAGACTGCCTCCCAGT	qRT-PCR
qpcr_hk_actin2_rev	AGGTCTTTTCTGACGTCGAC	qRT-PCR
5559_LB_ol_for	TTTCCCTAAACTCCCCCCACTGCAGCGAAGACCTTTGCTGTTCTC	PefD/mCherry fusion
5559_mcherry_ol_Pac1_rev	CCTCGCCCTTGCTTACCTTAATTAAGTTCTTCTTGCAGTGCTCCT	PefD/mCherry fusion
BB_mcherry_Pac1_for	TTAATTAAGGTAAGCAAGGGCG	PefD/mCherry fusion
BB_LB_PefD_rev	CTGCAGTGGGGGGAGTTT	PefD/mCherry fusion
5559_LB_ol_for	TTTCCCTAAACTCCCCCCACTGCAGCGAAGACCTTTGCTGTTCTC	PefD/GFP fusion
5559_cGFP_ol_Pac1_rev	CACCCTTGGAAACCATCTTAATTAAGTTCTTCTTGCAGTGCTCCT	PefD/GFP fusion
BB_cGFP_Pac1_for	TTAATTAAGATGGTTTCCAAGGGT	PefD/GFP fusion
BB_LB_PefD_rev	CTGCAGTGGGGGGAGTTT	PefD/GFP fusion
OL_olic(p)_SPpefD_fwd	CCATCACATCACAATCGATCCAACCATGAAGATCTCATTCGTTTTCGC	SP from PefD/GFP fusion
SPpefD_OL_GFP_rev	GATTACTTACCTCACCCTTGGAAACTCTTTTGACTGGAGTAGAGGG	SP from PefD/GFP fusion
OL_olic(p)_pefDwoSP_fwd	CCATCACATCACAATCGATCCAACCGCAGATATTGACTGCGAAAAGAC	PefD without SP/GFP fusion

Journal of Cell Science • Supplementary information

pefDwoSP_Olgfp_rev	GATTACTTACCTCACCCTTGGAAACGTTCTTCTTGCAGTGCTCCTC	PefD without SP/GFP fusion
olic(p)_2_rev	GGTTGGATCGATTGTGATGTGAT	GFP plasmid backbone
gfp_noATG_fwd	GTTTCCAAGGGTGAGGTAAG	GFP plasmid backbone
OL_eft-3p_pefD_fwd	AGTTGGGAAACACTTTGCTCACCGGTATGAAGATCTCATTCGTTTTCGC	PefD/mScarlet expression under *eft-3* promoter
OL_eft-3p_pefDnoSP_fwd	CAGTTGGGAAACACTTTGCTCACCGGTATGGTAGCAATTCCCTCTACTC	PefD/mScarlet expression under *eft-3* promoter
wrmscarlet_rev	CTTGTAGAGCTCGTCCATTCCTC	PefD/mScarlet expression under *eft-3* promoter
Peft3_rev	GAGCAAAGTGTTTCCCA	PefD/mScarlet expression under *eft-3* promotoe
5559LB-pjet-ol-for-n	GATGGCTCGAGTTTTTCAGCAAGATAACCTGCGTTAGTCGCGATT	Deletion of *pefD*
5559LB-H-ol-rev	TGACCTCCACTAGCATTACACTTTTTGATAGTATGAAAGTTTATATGGTT	Deletion of *pefD*
5559RB-H-ol-for	ATGCTCTTTCCCTAAACTCCCCCCAGATACAGATTTTGTTAAACTGCG	Deletion of *pefD*
5559RB-pjet-ol-rev-n	ATTGTAGGAGATCTTCTAGAAAGATTTAGAAGGCAGTCTTGACGG	Deletion of *pefD*
H-5559LB-ol-for	CCATATAAACTTTCATACTATCAAAAAGTGTAATGCTAGTGGAGGT	Deletion of *pefD*
H-5559RB-ol-rev	TCCGCAGTTTAACAAAATCTGTATCTGGGGGGAGTTTAGGGAAA	Deletion of *pefD*
5559ko_up_for_n	CTACCAAACTTCGAAGAAGG	analytic PCR deletion of *pefD*
5559ko_down_rev_nn	GAGCCCTCAATATTTCTGTAC	analytic PCR deletion of *pefD*
RB_pefD_fwd	GATACAGATTTTGTTAAACTGCGG	Southern blot analysis
RB_pefD_rev	TTAGAAGGCAGTCTTGACGGT	Southern blot analysis
OL_pJet_h2b(P)_fwd	GCTCGAGTTTTTCAGCAAGATGGATCCGGAGAAGAAAGGAGCAAAATCG	amplification of Nourseothricin resistence for recomplementation

tubA(T)_OL_pefD(p)_rev	AGAGAACAGCAAAGGTCTTCGCTGCAGGGATCCAGACAGCCAATTGAAA	amplification of Nourseothricin resistence for recomplementation
OL_pPF37BB_rab3P_fw	AGCGGATAACAATTTCACAGGGCCCGATCTTCAGATGGGAGCAGT	*rab-3*-promoter for *pefD* expression
rab3P_OL_pefD_rev	GAAAACGAATGAGATCTTCATACCGGTCTGAAAATAGGGCTACTGTAGA	*rab-3*-promoter for *pefD* expression
rab3P_OL_pefDdeltaSP_rev_neu	TCTTTTCGCAGTCAATATCTGCCATACCGGTCTGAAAATAGGGCTACTG	*rab-3*-promoter for *pefD* without SP expression
rab3(p)_rev	CATGATTTATTTTAAAAGAGCATTTAGATTAC	Plasmid backbone *rab-3*-promoter
unc-54_3UTR_fwd	GAGCTCCGCATCGGCCGC	Plasmid backbone *rab-3*-promoter
OL_rab3P_pefDnoSP_fwd	CTAAATGCTCTTTTAAAATAAATCATGGCAGATATTGACTGCGAAAAG	Expression of *pefD* without SP under *rab-3* promoter
pefD_OL_uncseq	TGATGACAGCGGCCGATGCGGAGCTCGTTCTTCTTGCAGTGCTCC	Expression of *pefD* under *rab-3*-promoter
OL_rab3(p)_nipA_fwd	AAATCTACAGTAGCCCTATTTTCAGATGAAAGGCGCTATCCTCATTAT	Expression of *nipA* under *rab-3*-promoter
OL_rab3(p)_nipAnoSP_fwd	AAATCTACAGTAGCCCTATTTTCAGATGCCGACCTCCAAAATATGC	Expression of *nipA* without SP under *rab-3*-promoter
nipA_OL_unc54UTR_rev	GATGACAGCGGCCGATGCGGAGCTCCTAGGCTTCCTCGTCGGG	Expression of *nipA* under *rab-3*-promoter
OL_rab3(p)_cyrA_fwd	AAATCTACAGTAGCCCTATTTTCAGATGCAGCTCCTCAGCACTATC	Expression of *cyrA* under *rab-3*-promoter
OL_rab3(p)_cyrAnoSP_fwd	AAATCTACAGTAGCCCTATTTTCAGATGAACCCCAATGTATACGACTC	Expression of *cyrA* without SP under *rab-3*-promoter
cyrA_OL_unc54UTR_rev	GATGACAGCGGCCGATGCGGAGCTCTTAGTAGCACTTTTCGCACAAAGT	Expression of *cyrA* under *rab-3*-promoter



Movie 1. Trapping of *C. elegans* by *A. flagrans*. Representative video showing *C. elegans* captured by adhesive three-dimensional trapping structures from *A. flagrans*. At first, it struggles in the trap, but then it is paralyzed and doesn´t move anymore. Video was taken for 11 hours, each 11 minutes a picture was taken with an AxioObserver.Z1 equipped with a Zeiss multi-Laser Module (488 nm diode laser and 561 nm OPSL laser), a spinning disk module CSU-X1M 5000 and an AxioCam MRm.



Movie 2. Movement of *C. elegans* expressing *pefD* pan-neuronal. Representative video showing locomotion of animals expressing PefD with and without signal peptide under the *rab-3* promoter and the wildtype N2. *pefD* and *pefDΔSP* expressing worms move slower than the wildtype N2. Recordings were made for 1 minute capturing images every second in the DIC channel at the SteREO Lumar V.12.

Journal of Cell Science • Supplementary information

References

Emser, J., N. Wernet, B. Hetzer, E. Wohlmann, and R. Fischer. 2024. The small cysteine-rich virulence factor NipA of *Arthrobotrys flagrans* interferes with cuticle integrity of *Caenorhabditis elegans*. *Nat Commun*. *15*:5795.

Pop, M., A.L. Klemke, L. Seidler, N. Wernet, P.L. Steudel, V. Baust, E. Wohlmann, and R. Fischer. 2024. Caenorhabditis elegans neuropeptide NLP-27 enhances neurodegeneration and paralysis in an opioid-like manner during fungal infection. *iScience*. 27:109484.

Wernet, N., V. Wernet, and R. Fischer. 2021. The small-secreted cysteine-rich protein CyrA is a virulence factor of *Duddingtonia flagrans* during the *Caenorhabditis elegans* attack. *PLoS Pathog*. 17:e1010028.

Wernet, V., J. Wäckerle, and R. Fischer. 2022. The STRIPAK component SipC is involved in morphology and cell-fate determination in the nematode-trapping fungus *Duddingtonia flagrans*. *Genetics*. 220:iyab153.

Journal of Cell Science • Supplementary information